

Controllable continuous-wave Nd:YVO₄ self-Raman lasers using intracavity adaptive optics

Ran Li,^{1,*} Mike Griffith,² Leslie Laycock,² and Walter Lubeigt¹

¹Centre for Microsystems and Photonics, Department of Electronic & Electrical Engineering, University of Strathclyde, Glasgow, G1 1XW, UK

²BAE Systems Advanced Technology Centre, West Hanningfield Road, Great Baddow, Chelmsford, CM2 8HN, UK

*Corresponding author: ran.li@strath.ac.uk

Received June 6, 2014; revised July 9, 2014; accepted July 11, 2014;

posted July 11, 2014 (Doc. ID 213664); published August 7, 2014

A controllable self-Raman laser using an adaptive optics (AO)-based control loop featuring an intracavity deformable mirror is reported. This method has the potential to alleviate thermal lensing within the Raman and laser gain media, and enable solid-state Raman lasers to reach new power levels. A proof-of-concept experiment using a Nd:YVO₄ self-Raman laser and resulting in 18% enhancement of the first Stokes output power is reported. Moreover, wavelength selection between two Raman laser outputs ($\lambda = 1109$ and 1176 nm) emanating from the 379 and 893 cm⁻¹ Raman shifts of YVO₄, respectively, was achieved using this AO technique. © 2014 Optical Society of America

OCIS codes: (010.1080) Active or adaptive optics; (140.3550) Lasers, Raman; (140.3580) Lasers, solid-state; (140.3530) Lasers, neodymium; (140.6810) Thermal effects.

<http://dx.doi.org/10.1364/OL.39.004762>

Stimulated Raman scattering (SRS) is widely recognized as a practical and efficient approach to extend the spectral coverage of solid-state lasers operating in the near-infrared and visible spectra, especially when SRS is combined with second-harmonic generation or sum frequency generation [1–3]. However, the nonelastic nature of SRS results in the dissipation of a significant portion of energy as heat in the Raman material. This inevitably leads to undesired thermo-optical distortions and impacts the performance of the Raman laser (especially when the Raman crystal is inserted within the laser cavity). This additional thermal lensing scales directly with the Raman laser output power and has been identified as the main limitation in power scaling crystalline Raman lasers operating in the continuous-wave (CW) regime [2,4]. The use of low-loss, low-birefringence synthetic diamond can significantly reduce the effects of SRS-induced thermal lensing in CW Raman lasers [5–7]. In this Letter, we propose a method to reduce the effects of both SRS and laser-induced thermal lensing, leading to power scaling of crystalline Raman lasers. This method is based on a feedback control loop using adaptive optics (AO), which has been used to optimize the performance of solid-state lasers by compensating for the thermal lens effect within the laser gain medium [8–10].

In this Letter, the proof-of-concept implementation of this technique inside a crystalline Raman laser is reported for the first time to our knowledge. A bimorph deformable mirror (DM) was inserted as the end mirror in a self-Raman Nd:YVO₄ laser cavity. In this so-called self-Raman configuration, laser conversion and SRS occurred within the same Nd:YVO₄ crystal, which in turn became the subject of intense thermal buildup. Consequently, this self-Raman configuration was believed to be an ideal test bed to implement this feedback loop. In addition to power enhancement, this AO-based system was also used to control the wavelength of the output beam by selecting the Raman transitions of the YVO₄ crystal used in this laser.

The experimental setup, shown in Fig. 1, was built to optimize the first Stokes output power of the Nd:YVO₄ laser emitting at $\lambda = 1176$ nm. In addition to the intracavity DM, the AO feedback loop included a photodiode sensor to detect the Raman output intensity and a PC-based control program featuring a search algorithm. The 18-mm-diameter DM contained 37 piezoelectric actuators distributed in a radial pattern over an active aperture of 15 mm (see Fig. 2). Individual voltages were supplied to the mirror actuators using a multichannel digital-to-analog converter and a multichannel high-voltage amplifier. Using a Shack–Hartmann wavefront sensor-based system, the focusing power of the DM along x axis, as defined in Fig. 2, was measured to range linearly from -0.74 to 1.03 D when a voltage of -50 to 250 V was applied to all actuators, respectively. Likewise, the focusing power of the DM along y axis ranged from -0.61 to 1.33 D. The random search algorithm described in [8] was integrated within the control program written using National Instruments Labview. This search algorithm aimed to find the DM shape providing the optimum signal recorded by the photodiode. As described in [11], this algorithm was tailored to reduce the effect of the long-term output power variation experienced in this type of high-power laser systems. In addition, only the central seven actuators were used in the algorithm to speed up the search procedure. In this way, the DM shape providing the optimum Raman output intensity was approached

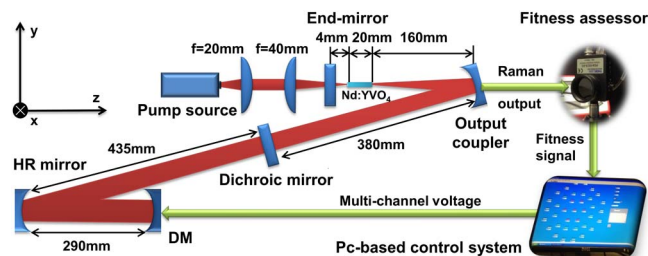


Fig. 1. Diagram of the Nd:YVO₄ self-Raman laser incorporating the AO feedback loop.

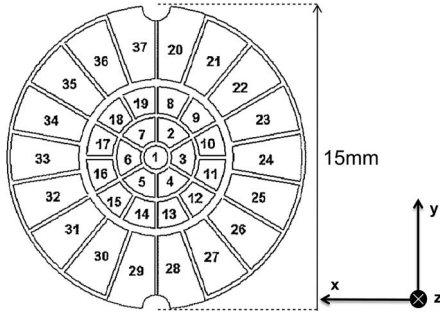


Fig. 2. Actuator designation of the DM.

by the program. A fiber-coupled laser diode (100 μm core diameter, NA ~ 0.22) capable of producing up to 32 W pump power at $\lambda = 880$ nm was used to pump the gain medium. Two plano-convex lenses were used to re-image a 100 μm beam waist at the center of the crystal. An a-cut, 20-mm-long (2-mm-diameter), 0.3 at. % doped Nd:YVO₄ rod was mounted in a water-cooled copper block and was used as the laser and Raman gain medium. Its side surfaces were antireflection-coated [reflectivity (R) $< 0.1\%$ at $\lambda = 1064$ and 1109–1176 nm; $R < 5\%$ at $\lambda = 880$ nm]. An $\times 4$ intracavity telescope ensured a ~ 1.5 mm diameter laser spot on the DM to maximize its effects on the intracavity laser field. The four-mirror laser cavity for the fundamental radiation was composed of a flat end mirror, a concave [radius of curvature (ROC) = 1 m] high-reflectivity mirror (both coated with $R > 99.95\%$ at $\lambda = 1064$ and 1109–1176 nm), the DM ($R > 99.9\%$ at $\lambda = 1064$ nm), and a strongly concave (ROC = 0.25 m) output coupler [$R > 99.97\%$ at $\lambda = 1064$ nm, transmission (T) = 1% at $\lambda = 1176$ nm, $T \sim 0.2\%$ at $\lambda = 1109$ nm]. Since the DM was not coated for the first Stokes wavelength, a flat dichroic mirror ($R < 1\%$ at $\lambda = 1064$ nm and $R > 99.98\%$ at $\lambda = 1109$ and 1176 nm) was used as the end mirror for the first Stokes Raman laser cavity. This dichroic mirror was placed 380 mm away from the output coupler to optimize the mode match between the fundamental and Raman laser beams within the Nd:YVO₄ crystal. The DM was placed so that its x axis, as defined in Fig. 2, and the optical propagation axis were contained within the horizontal plane.

With no voltage applied to the DM, the laser was aligned to deliver a maximum Raman output power of 500 mW for an absorbed laser diode pump power of 10.8 W. In this case, the focal length of the first order of the thermal lens (f_{thl}) present in the Nd:YVO₄ crystal could be estimated to be ~ 50 mm. Using an ABCD-matrix software, the fundamental transverse mode radii of the fundamental ($\lambda = 1064$ nm) and Raman ($\lambda = 1176$ nm) laser fields at the center of the gain medium with and without thermal lensing are shown in Table 1. Only the radius of the Raman field was impacted by thermal lensing with a $\sim 20\%$ increase.

Then, a pre-optimization experiment was undertaken when all actuators were adjusted simultaneously. The Raman laser was found to operate only between 60 and 180 V corresponding to focusing powers of ~ 0 to ~ 0.80 D, respectively. The mirror shape delivering the optimum Raman output power (550 mW) was obtained for a

Table 1. TEM₀₀ Mode Radius at the Center of the Gain Medium for the Fundamental ($\lambda = 1064$ nm) and Raman ($\lambda = 1176$ nm) Fields with and without Thermal Lensing

	No Thermal Lensing	With $f_{\text{thl}} = 50$ mm
Fundamental laser mode radius along x axis (μm)	101	101
Fundamental laser mode radius along y axis (μm)	95	95
Raman laser mode radius along x axis (μm)	102	119
Raman laser mode radius along y axis (μm)	103	119

voltage value of 112.5 V applied to all actuators (i.e., the focusing powers of the DM along x and y axes were 0.27 and 0.50 D, respectively). In this way, the TEM₀₀ mode radius of the fundamental laser field increased by $\sim 20\%$ (121 μm along x axis and 116 μm along y axis) and resulted in a near-perfect mode matching with the Raman laser field at the center of the gain medium. The beam quality M^2 factor of the Raman laser output beam was similar for both transverse axes and measured less than 1.1 and 1.4 for the first Stokes output and the fundamental laser beam, respectively. Using this DM shape, the optical power transfer of the Raman laser was measured (see Fig. 3). Then, an optimization procedure consisting of 42 actuator changes (which corresponded to a search duration of 5 min) returned a DM shape enabling a Raman laser output power of 650 mW, resulting in a power improvement of $\sim 18\%$. The beam quality M^2 factors along both x and y transverse axes measured less than 1.1 for the first Stokes laser output and 1.2 for the fundamental laser beam. Using a Shack–Hartman sensor, the wavefront correction induced by the DM shape before and after the search procedure was measured and the resulting Zernike coefficients are shown in Table 2.

In addition to power scaling, this AO-based technique was also used as a means to select the wavelength of the Nd:YVO₄ Raman laser. Neodymium-doped orthovanadates, such as Nd:YVO₄ and Nd:GdVO₄, have been shown to feature several Raman transitions [12] leading to the development of Raman lasers based on secondary Raman transitions [13–15]. Here, the AO system was used to rapidly modify the dynamics of the intracavity

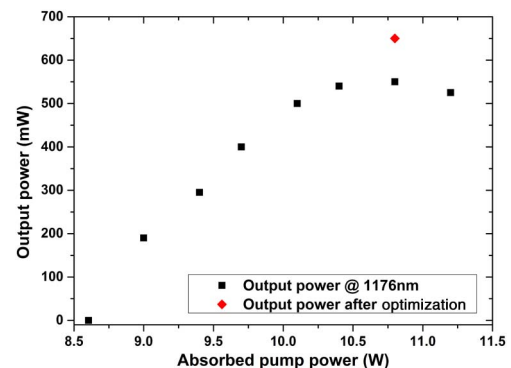


Fig. 3. Power transfer of the $\lambda = 1176$ nm output before optimization, including the post-optimization result.

Table 2. Zernike Coefficients before and after Power Scaling Investigation

Zernike Coefficient Order	Starting Point (μm)	End Point (μm)	Error Range (μm)
1 (piston)	-18.59	-18.49	0.01
2 (tip y)	14.79	14.76	0.01
3 (tip x)	3.87	3.78	0.01
4 (astigmatism $\pm 45^\circ$)	0.019	0.016	0.002
5 (defocus)	-0.125	-0.118	0.002
6 (astigmatism $\pm 0^\circ$)	0.055	0.071	0.002
7 (trefoil y)	-0.001	-0.004	0.001
8 (coma x)	-0.004	-0.006	0.001
9 (coma y)	0.002	0.011	0.001
10 (trefoil x)	-0.002	-0.005	0.001

laser field, resulting in a switch between the primary (893 cm^{-1}) and secondary (379 cm^{-1}) Raman transitions of the Nd:YVO₄ crystal. In this experiment, the laser cavity in Fig. 1 was slightly modified with the distance between the DM and the ROC = 1 m curved mirror set to 300 mm. At first, the laser resonator was aligned manually to only use the 379 cm^{-1} Raman shift with the DM actuators set at 0 V (i.e., focusing powers along x and y axes measured at -0.47 and -0.28 D , respectively), resulting in a 275 mW Raman laser output at $\lambda = 1109\text{ nm}$ for an absorbed laser diode pump power of 8.2 W . The beam quality M^2 factors along x and y transverse axes were measured to be 1.3 and 1.6 for the $\lambda = 1109\text{ nm}$ laser output. Using an optical spectrum analyzer (Agilent 86140B), the full width at half-maximum (FWHM) linewidth of the first Stokes output ($\lambda = 1109\text{ nm}$) can be estimated at 0.15 nm at a resolution of 0.06 nm . The optical power transfer at $\lambda = 1109\text{ nm}$ was measured as shown in Fig. 4. At a pump power of 10.1 W , $\sim 100\text{ mW}$ of the $\lambda = 1176\text{ nm}$ Raman output could also be observed in addition to the $\lambda = 1109\text{ nm}$ line. The surface of the DM was then changed to an approximately flat shape by applying a voltage of 66 V to all actuators. In this way, the primary (893 cm^{-1}) Raman shift was favored to the detriment of the 379 cm^{-1} shift. So, only the Raman laser at $\lambda = 1176\text{ nm}$ could be observed with an output power of 340 mW and with beam quality M^2 factors along x and y transverse axes measuring less than 1.1. The resulting FWHM linewidth of this Raman laser output was measured at 0.15 nm at a resolution of 0.06 nm . The optical power transfer of the $\lambda = 1176\text{ nm}$ output obtained with

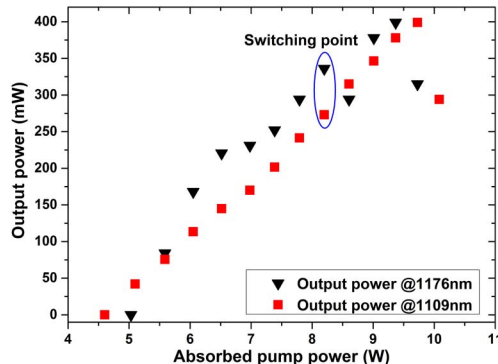


Fig. 4. Power transfer of Raman lasers resulting from the 379 cm^{-1} transition (in red) and the 893 cm^{-1} transition (in black).

the flat DM shape was measured as shown in Fig. 4. Again, at high pump powers (9.7 W), both Raman outputs could be observed with up to 100 mW of the $\lambda = 1109\text{ nm}$ output. The Zernike coefficients before and after the wavelength switch are shown in Table 3.

These two distinct experiments raise several discussion points.

Although the same DM was used in both investigations, the correction required to achieve the objective varied significantly. In the power scaling investigation, the correction range of the DM had to be limited to avoid any Raman laser modal collapse, which can occur if a strong curvature change to the DM drives the laser cavity outside its stability range [8]. As shown in Table 2, a high-order correction (mainly astigmatism and coma) was required to optimize the Raman output power since the first order of the thermal lens had mainly been compensated using the pre-optimization experiment. Meanwhile, in the wavelength selection experiment, a comparison of the Zernike coefficients expressed in Table 3 shows a significant variation in the defocus term (Z_5). Using this term along with the astigmatism term (Z_6), it is possible to calculate the radii of curvatures ROC_x and ROC_y of the DM shape as [16]

$$Z_{5x} = Z_5 + \frac{Z_6}{\sqrt{2}}, \quad (1)$$

$$Z_{5y} = Z_5 - \frac{Z_6}{\sqrt{2}}, \quad (2)$$

$$\text{ROC}_x = \frac{-\Phi_x^2}{8\sqrt{3}Z_{5x}}, \quad (3)$$

$$\text{ROC}_y = \frac{-\Phi_y^2}{8\sqrt{3}Z_{5y}}, \quad (4)$$

where Z_{5x} and Z_{5y} denote the defocus terms for x and y axes, respectively, and Φ_x and Φ_y are the diameters of the pupil along x and y axes, respectively (both diameters were 3 mm). Therefore, to favor the $\lambda = 1109\text{ nm}$ output, the ROCs of the DM surface along x and y axes

Table 3. Summary of Zernike Coefficients for Wavelength Control

Zernike Coefficient Order	Starting Point (μm)	End Point (μm)
1 (piston)	-19.32	-18.99
2 (tip y)	15.38	15.06
3 (tip x)	3.77	3.83
4 (astigmatism $\pm 45^\circ$)	0.016	0.016
5 (defocus)	0.121	-0.013
6 (astigmatism $\pm 0^\circ$)	0.043	0.048
7 (trefoil y)	0.002	0.001
8 (coma x)	-0.001	-0.003
9 (coma y)	0.004	0.002
10 (trefoil x)	0.003	0.001

were measured to be -4.29 and -7.17 m, respectively, whereas to obtain the $\lambda = 1176$ nm line, ROCs of >30 m and 13.8 m, respectively, were required for x and y axes. Using the ABCD-matrix software, this cylindrical curvature variation of the DM surface was found to increase the fundamental transverse mode of the $\lambda = 1064$ nm laser in the gain medium by $\sim 15\%$. So it can be concluded that optimal power scaling would require a DM with a moderate stroke and a large number of actuators, whereas wavelength selection could be best achieved using a DM with a lower number of actuators and a larger stroke.

In Fig. 3, the power transfer recorded prior to Raman output power optimization displays a distinct rollover commensurate with thermal lensing at pump powers above 10.4 W. The optimized Raman laser output power recorded for a pump power of 10.8 W is in line with the linear trend displayed for lower pump powers. Therefore, the disappearance of the rollover behavior makes us believe that the AO-control loop has significantly reduced the effect of thermal lensing within the Nd:YVO₄ crystal. In addition, the use of a bespoke random search algorithm was an attempt to conciliate speed with performance. More advanced algorithms would be required to improve the efficacy of this feedback loop.

In the wavelength control investigation, both Raman outputs could be observed simultaneously at pump powers above 9.5 W. Further investigation would be required to explain this Raman mode competition. However, it must be noted that the sum of their intensity meant that the total Raman output power was in line with the trend observed from lower powers.

In conclusion, for the first time to our knowledge, intracavity AO has been implemented inside a solid-state Raman laser to automatically increase the power and control the wavelength of the Raman output beam. The feedback control loop used for power scaling featured a DM, a photodiode sensor, and a PC-based control program using a random search algorithm. The use of this control loop resulted in an 18% improvement of the Raman laser output power of an end-pumped Nd:YVO₄ self-Raman laser emitting at $\lambda = 1176$ nm. This proof-of-concept experiment demonstrates the potential

of intracavity AO to alleviate the detrimental effects of thermal lensing and open avenues for power scaling of CW and high-average-power crystalline Raman lasers. In addition, wavelength control between $\lambda = 1109$ and 1176 nm has been achieved using this AO technique based on the 379 and 893 cm⁻¹ Raman shifts of YVO₄. This experiment paves the way toward automatic wavelength selectable high-power Raman lasers.

This work has been supported by the UK EPSRC (grant number EP/K009982/1).

References

1. P. Cerny, H. Jelinkova, P. G. Zverev, and T. T. Basiev, *Prog. Quantum Electron.* **28**, 113 (2004).
2. J. A. Piper and H. M. Pask, *IEEE J. Sel. Top. Quantum Electron.* **13**, 692 (2007).
3. H. M. Pask, P. Dekker, R. P. Mildren, D. J. Spence, and J. A. Piper, *Prog. Quantum Electron.* **32**, 121 (2008).
4. A. J. Lee, H. M. Pask, D. J. Spence, and J. A. Piper, *Opt. Lett.* **35**, 682 (2010).
5. W. Lubeigt, G. M. Bonner, J. E. Hastie, M. D. Dawson, D. Burns, and A. J. Kemp, *Opt. Lett.* **35**, 2994 (2010).
6. V. G. Savitski, I. Friel, J. E. Hastie, M. D. Dawson, D. Burns, and A. J. Kemp, *IEEE J. Quantum Electron.* **48**, 328 (2012).
7. O. Kitzler, A. McKay, and R. P. Mildren, *Opt. Lett.* **37**, 2790 (2012).
8. W. Lubeigt, G. Valentine, and D. Burns, *Opt. Express* **16**, 10943 (2008).
9. P. Yang, X. Lei, R. Yang, M. Ao, L. Dong, and B. Xu, *Appl. Phys. B* **100**, 591 (2010).
10. S. Piehler, B. Weichelt, A. Voss, M. A. Ahmed, and T. Graf, *Opt. Lett.* **37**, 5033 (2012).
11. W. Lubeigt, S. P. Poland, G. J. Valentine, A. J. Wright, J. M. Girkin, and D. Burns, *Appl. Opt.* **49**, 307 (2010).
12. A. A. Kaminskii, K. Ueda, H. J. Eichler, Y. Kuwano, H. Kouta, S. N. Bagaev, T. H. Chyba, J. C. Barnes, G. M. A. Gad, T. Murai, and J. Lu, *Opt. Commun.* **194**, 201 (2001).
13. F. Shuzhen, Z. Xingyu, W. Qingpu, L. Zhaojun, L. Lei, C. Zhenhua, C. Xiaohan, and Z. Xiaolei, *Opt. Commun.* **284**, 1642 (2011).
14. J. Lin and H. M. Pask, *Opt. Express* **20**, 15180 (2012).
15. R. Li, R. Bauer, and W. Lubeigt, *Opt. Express* **21**, 17745 (2013).
16. D. Malacara, *Optical Shop Testing*, 2nd ed. (Wiley, 1992).